Characterization and Parasitic Extraction of EMI Filters Using Scattering Parameters

Shuo Wang, *Student Member, IEEE*, Fred C. Lee, *Fellow, IEEE*, and Willem Gerhardus Odendaal, *Member, IEEE*

***Abstract*—In this paper, the electromagnetic interference (EMI) filter is first characterized using Scattering parameters (S-parameters). Based on this S-parameters model, the insertion voltage gains are derived for EMI filter with arbitrary levels of source and load impedances. Experiments are carried out to verify this approach. Based on the network theory, S-parameters are then utilized to extract the parasitic couplings in both one-stage and two-stage EMI filters. EMI filter models are constructed. Experiments finally verify the proposed methods. The approaches are very useful for the prediction of EMI filter performance, and for the design and optimization of EMI filters.**

***Index Terms*—Electromagnetic interference (EMI) filter, insertion loss, insertion voltage gain, parasitic coupling, scattering parameters, Tee network.**

I. Introduction

ELECTROMAGNETIC interference (EMI) filters are widely used in power electronics area. Traditionally, electromagnetic interference (EMI) filters are characterized by the insertion loss that occurs when both source and load impedances are 50 Ω. However, in a practical filter implementation, source and load cannot both be 50 Ω; this makes it difficult to base EMI filter selection on the curves provided by manufacturers. In order to efficiently predict their performance, EMI filters should be characterized by independent network parameters.

On the other hand, an efficient network parameter is needed to extract the parasitics in EMI filters. It is shown that electromagnetic couplings among filter components and circuit layouts play very important roles in the high frequency (HF) performance of EMI filters [9]. Although EMI filter performance is also affected by the parasitic parameters of the components, including the equivalent series inductor (ESL) of the capacitors and the equivalent parallel capacitor (EPC) of the inductors, for many cases, especially at HF range, these factors may be less important than the couplings among components and layouts. A typical differential-mode (DM) EMI filter used for power converters is shown in Fig. 1, where DM inductance L is the leakage inductance of the coupled common-mode (CM) inductor. In Fig. 2 two insertion voltage gain curves of this filter are compared. One is the simulated curve using the model including only the component parasitic parameters [10]; and the other is the measured curve. Obviously, the measured one is much worse than the simulated one. Therefore it is necessary to carry out a detailed study of the parasitic couplings. The effects of parasitic couplings on EMI filter performance are discussed in detail in another paper [9]. Fig. 3 shows a model that includes all these couplings: basically, they can be divided into five categories as follows.

1) Coupling between inductor and capacitors: M_1 and M_2.
2) Coupling between two capacitors: M_3.
3) Coupling between inductor and trace loops: M_4 and M_5.
4) Coupling between ground plane and inductor: M_7 and $C_{\rm p}$.
5) Coupling between trace loops: M_6.

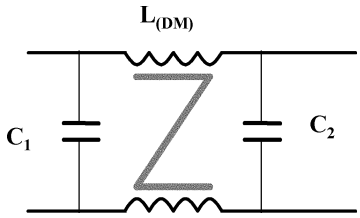

Fig. 1. Investigated one-stage DM EMI filter.

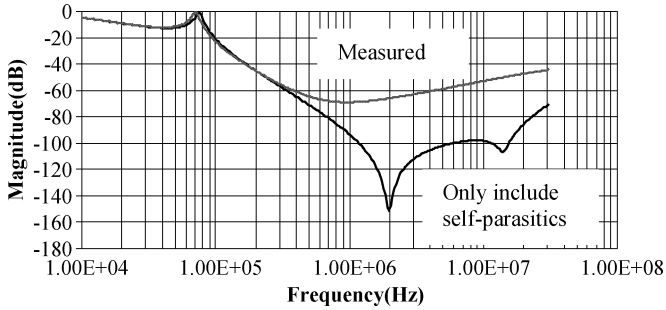

Fig. 2. Comparison of insertion voltage gains when both source and load are 50 Ω.

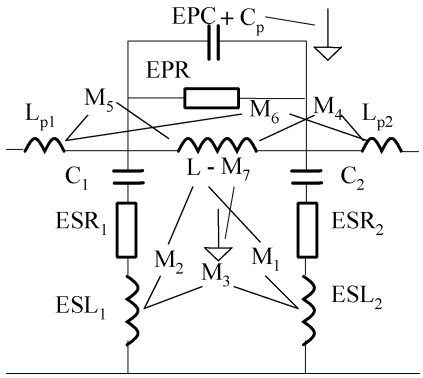

Fig. 3. Parasitic couplings in an EMI filter.

Manuscript received February 2, 2004; revised August 18, 2004. Recommended by Associate Editor F. Blaabjerg.

The authors are with the Bradley Department of Electrical and Computer Engineering, Virginia Polytechnic Institute and State University, Blacksburg, VA 24061 USA (e-mail: shwang6@vt.edu).

Digital Object Identifier 10.1109/TPEL.2004.842949

Air is the medium for all these parasitic couplings. M_1, M_2, M_4, M_5, and M_7 are much smaller than the inductance L of the inductor, so the effects of these couplings on the inductance L are negligible. The effects of parasitic couplings on the capacitors are superposed because the media of these couplings are linear. For these two reasons, these parasitic parameters can be considered independent from each other, so it is possible to extract them separately. These parasitic parameters are difficult to extract using conventional methods. It is impractical to calculate them using electromagnetic software because of the complicated structures of capacitors and inductors. It is also impossible to directly measure them using an impedance analyzer because they are mutual couplings between two components. However, these parasitic parameters can be calculated from measured network parameters based on the network theory, as will be shown in this paper.

Scattering parameters (S-parameters) are chosen to characterize EMI filters [11] and to extract mutual couplings because of two reasons. First, in the HF range, they are easier to accurately measure than it is to do so for the $[Z]$, $[Y]$, $[H]$, and $[ABCD]$ parameters. The measurement of $[Z]$, $[Y]$, $[H]$ and $[ABCD]$ parameters requires either a short circuit or an open circuit at one port, which is difficult to achieve in the HF range because of parasitic parameters [1], [2], [8]; for S-parameters, no short or open circuits are needed for measurement. Second, interconnect parasitics make measurements inaccurate at high frequencies. The S-parameter method can be calibrated to the exact points of measurement, thus excluding the effects of parasitics that occur due to measurement interconnects [3], [4], [6].

II. Using S-Parameters to Characterize EMI Filters

A. Characterization of EMI Filters Using S-Parameters

Strictly speaking, an EMI filter is not a linear network because it contains nonlinear components such as inductors; however, it is approximately linear for a small-signal excitation. So it is reasonable to characterize an EMI filter as a linear, passive, two-port network under small-signal excitation conditions. The nonlinear characteristics can be modeled with the current biases superposed by a small-signal excitation. The test setup for an EMI filter is shown in Fig. 4, where the EMI filter is characterized in terms of waves. There are four waves in Fig. 4, namely, incident wave a_1 and reflected wave b_1 at port1, and incident wave a_2 and reflected wave b_2 at port2. From these four variables, the voltage[1] V_1 and current I_1 at port1 and the voltage V_2 and current I_2 at port2 are found by (1)–(4) [2], where Z_0 is the reference impedance, which is usually real 50 Ω

$$V_1 = \sqrt{Z_0}(a_1 + b_1); \tag{1}$$

$$V_2 = \sqrt{Z_0}(a_2 + b_2); \tag{2}$$

$$I_1 = \frac{1}{\sqrt{Z_0}}(a_1 - b_1) \qquad \text{and} \tag{3}$$

$$I_2 = \frac{1}{\sqrt{Z_0}}(a_2 - b_2). \tag{4}$$

To fully characterize a linear, passive, two-port network, two linear equations are required among the four wave variables [5].

[1]All currents and voltages are RMS values.

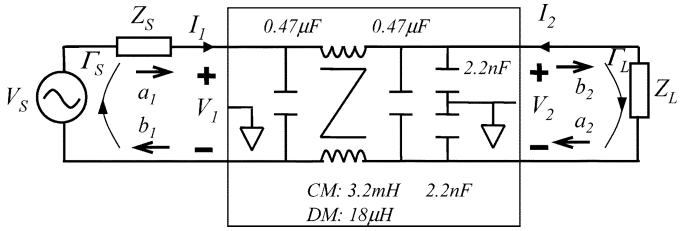

Fig. 4. EMI filters are treated as linear, passive, two-port networks under small-signal excitation conditions. V_S: voltage source; Z_S: source impedance; Z_L: load; a_1, a_2: normalized incident wave on source side and load side, respectively; b_1, b_2: normalized reflected wave on source side and load side, respectively; I_1, I_2: input current of port1 and port2, respectively; V_1, V_2: voltage of port1 and port2, respectively.

The four S-parameters in (5) are therefore introduced to correlate with a_1, a_2, b_1 and b_2 [8]. S_{11} and S_{22} are called reflection coefficients. S_{12} and S_{21} are called transmission coefficients. When reflected wave b_1 or b_2 reaches the source or load side, it would be reflected because of the mismatched impedances. The reflection coefficients, Γ_S at the source side and Γ_L at the load side, are given by

$$\begin{pmatrix} b_1 \\ b_2 \end{pmatrix} = \begin{pmatrix} S_{11} & S_{12} \\ S_{21} & S_{22} \end{pmatrix} \begin{pmatrix} a_1 \\ a_2 \end{pmatrix} \tag{5}$$

$$\Gamma_S = \frac{Z_S - Z_0}{Z_S + Z_0} \qquad \text{and} \tag{6}$$

$$\Gamma_L = \frac{Z_L - Z_0}{Z_L + Z_0}. \tag{7}$$

From (1)–(7), the insertion voltage gain (the reciprocal of insertion loss) of EMI filters with arbitrary levels of source and load impedances can be found by (8)

$$A_V = \frac{S_{21}(1 - \Gamma_L\Gamma_S)}{(1 - S_{11}\Gamma_S)(1 - S_{22}\Gamma_L) - S_{21}\Gamma_L S_{12}\Gamma_S}. \tag{8}$$

Note that the insertion voltage gain is defined as the ratio of the port voltage at the load side without the filter to that with the filter [1], which is different from the input-to-output voltage gain. From (8), as long as the S-parameters of an EMI filter are measured, the insertion voltage gain (or insertion loss) for an arbitrary Z_S and Z_L can be found. Term Z_S can be found using a method described in other work [7]. It is obvious that the source and load impedances affect the insertion voltage gain through reflection coefficients Γ_S and Γ_L.

B. Experiments

Two experiments are carried out for the EMI filter in Fig. 4. In the first experiment, in order to investigate the effects of noise source impedance on EMI filter performance, an inductor shown as in Fig. 5 is used as the DM noise source. The load is 100 Ω. The predicted insertion voltage gain, the measured insertion voltage gain, and the measured 50 Ω-based transfer gain (reciprocal of 50 Ω-based insertion loss) of the DM filter part are all shown in Fig. 6. The prediction very closely matches the measurement. It is obvious that the transfer-gain curve from a 50 Ω-based measurement system is quite different from the practical insertion voltage gain. So the transfer-gain curve (50 Ω-based insertion loss) does not offer accurate information

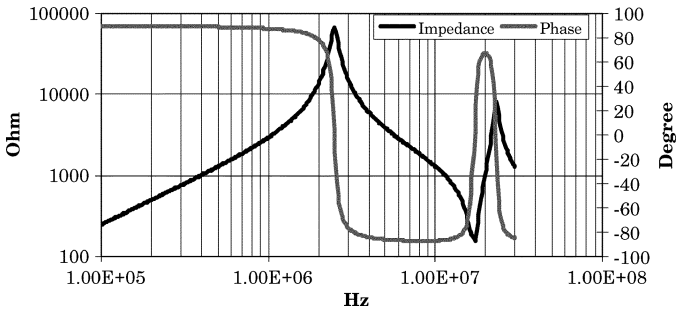

Fig. 5. Impedance of the inductor used as DM source.

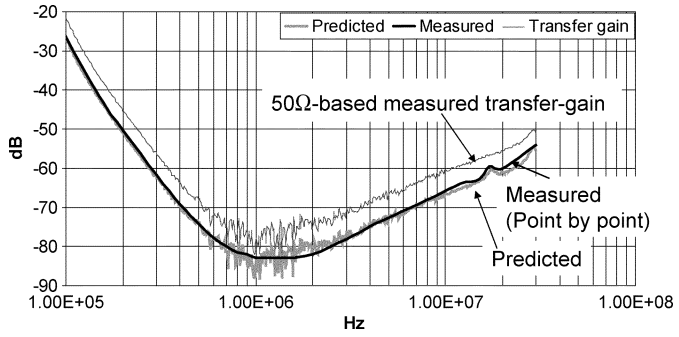

Fig. 6. Comparison of the predicted insertion voltage gain, the measured insertion voltage gain, and the measured 50 Ω-based transfer gain.

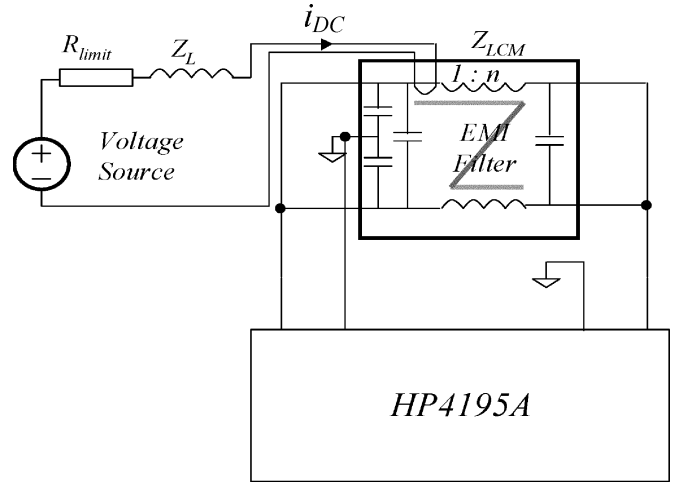

Fig. 7. S-parameter measurement setup for the CM filter part.

on filter performance. The small peak of the insertion voltage gains between 10 MHz and 20 MHz is caused by the corresponding valley of the source impedance shown in Fig. 5.

In the second experiment, in order to investigate the effects of CM current on the EMI filter performance, the CM, dc current bias is injected through a one-turn auxiliary winding on the CM inductor, as shown in Fig. 7. If the turn ratio of CM windings to the auxiliary winding is n, the equivalent CM current bias is $i_{\rm DC}/n$. Because of the high turn ratio and the high impedance Z_L, the effects of the dc current loop is ignored. Both DM and CM filter parts are measured in the experiments. For the CM filter part, the final measurement results show that the S-parameters changed significantly when the equivalent CM current bias is increased from 0 A to 0.2 A. This is due to the saturation of

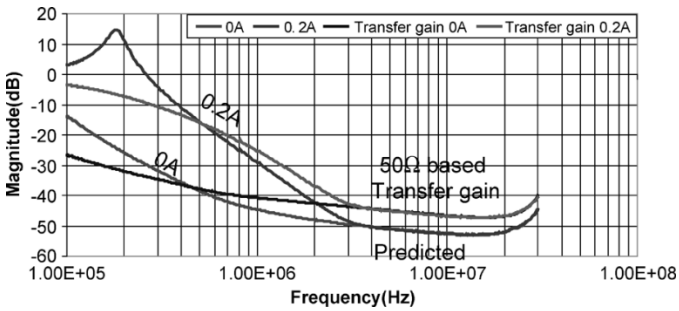

Fig. 8. Predicted insertion voltage gains for the CM filter part ($Z_S = 100$ pF, $Z_L = 25\ \Omega$).

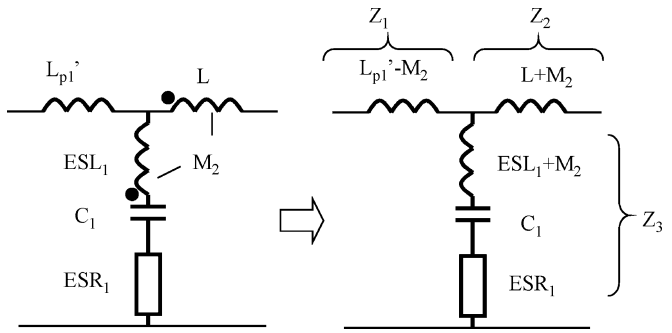

Fig. 9. Calculation of M_2 through the impedance of the capacitor branch.

the CM inductor. On the other hand, experiment shows CM current bias has no significant effect on DM filter performance for the investigated EMI Filter. Fig. 8 shows the predicted CM filter performance with 100 pF source impedance and 25-Ω load. In the HF range, saturation of the core has no effect on the insertion voltage gain because the HF noise comes through parasitic paths instead of the inductor path. The peak on the curve of 0.2 A between 100 kHz and 200 kHz could not be estimated just from the 50 Ω-based transfer-gain curve. In a practical EMI filter design, measures should be taken to prevent the saturation of the CM inductors. For example, the CM capacitors between the CM inductor and the converter should be sufficiently large that they can bypass enough CM current so as to prevent a large level of CM current from saturating the CM inductor.

III. Using S-Parameters to Extract Parasitic Parameters

A. Network Theory

In Fig. 3, the mutual inductances exist between two components, so it is impossible to measure them separately. Measurement can be carried out for the network that includes two components, and then the mutual inductance can be derived from the measured data. As an example, mutual inductance M_2, which is shown in Fig. 9, can be calculated from the impedance of the capacitor branch.

In Fig. 9, the parasitic parameters of the inductor are ignored because they are insignificant in the low-frequency range. For the mutual coupling between the inductor and the capacitor, the decoupled model is shown on the right. The inductance of the

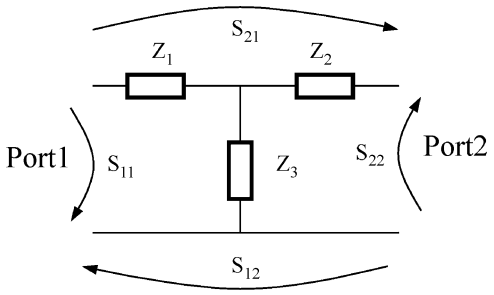

Fig. 10. S-parameters of a Tee network.

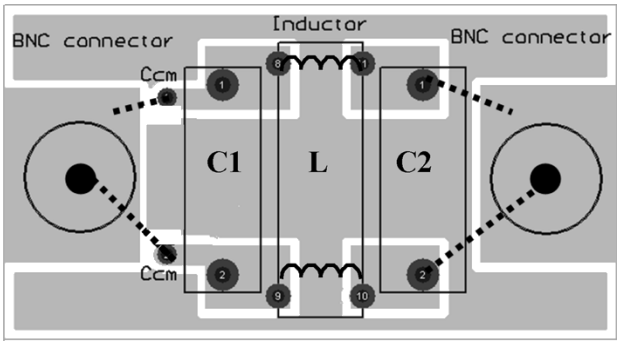

Fig. 11. PCB layout of the investigated one-stage DM EMI filter.

capacitor branch is changed by M_2. M_2 can therefore be calculated from the difference between the impedances of the capacitor branch with and without the coupling. S-parameters are first calibrated and measured from port1 and port2, and then the impedance of the capacitor branch is calculated from measured S-parameters, and finally M_2 can be found.

The decoupled model in Fig. 9 is in fact a Tee network as shown in Fig. 10. Based on the relationship between impedances and S-parameters, three impedances in the Tee network can be calculated from the measured S-parameters

$$Z_1 = \frac{Z_0\left(1-S_{22}-S_{22}S_{11}+S_{11}-2S_{21}+S_{21}^2\right)}{\left(1-S_{22}+S_{22}S_{11}-S_{11}-S_{21}^2\right)} \tag{9}$$

$$Z_2 = \frac{Z_0\left(1+S_{22}-S_{22}S_{11}-S_{11}-2S_{21}+S_{21}^2\right)}{\left(1-S_{22}+S_{22}S_{11}-S_{11}-S_{21}^2\right)} \quad \text{and} \tag{10}$$

$$Z_3 = \frac{2Z_0S_{21}}{\left(1-S_{22}+S_{22}S_{11}-S_{11}-S_{21}^2\right)}. \tag{11}$$

From (11), as long as the S-parameters are measured, impedance Z_3 of the capacitor branch can be calculated, and then M_2 can be found. Most of parasitic parameters in the EMI filter can be calculated using this proposed method.

B. Extraction of Parasitic Parameters for a One-Stage EMI Filter

The printed circuit board (PCB) layout of the one-stage DM filter in Fig. 1 is shown in Fig. 11. In experiments, HP 4195A is used to measure S-parameters. HP 4195A is designed for single-ended measurement; however, the DM EMI filter in Fig. 1 is a balanced structure. In order to solve this problem, two inductor windings are reconnected in series on one side of the filter, and the other side of the filter is grounded, which makes the filter a single-ended structure, as shown in Fig. 12. Because the inductor current, winding structure and inductor

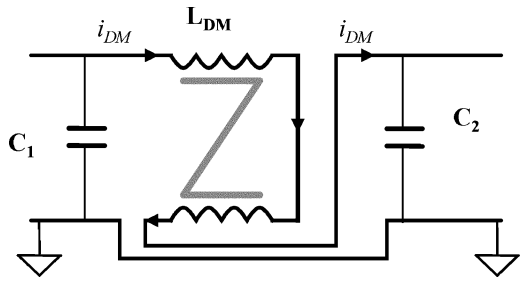

Fig. 12. DM EMI filter is connected to a single-ended structure.

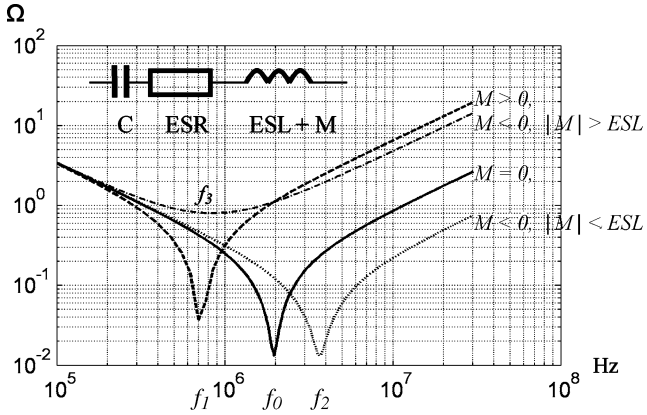

Fig. 13. Calculated impedances for a capacitor branch with different mutual inductances.

position on the PCB are kept the same, the extracted couplings of the filter will be the same as those of the balanced structure. The frequency is swept from 150 kHz to 30 MHz.

1) Extraction of M_1, M_2, M_4 and M_5 in Fig. 3: In order to extract M_1 or M_2 separately, other couplings should be kept as small as possible. In the measurement, only a capacitor and the inductor are kept on the PCB, so the couplings caused by other components are excluded. In and out trace loops of the filter are reduced very small so that the couplings between trace loops and other components will be negligible. In Fig. 9, L'_{p1} and L'_{p2} are the inductances of the modified trace loops. Because mutual inductance is to be derived from the impedance of the capacitor branch, it is necessary first to investigate the effects of these couplings on the impedance of the capacitor branch.

A general case for the capacitor branch is shown in Fig. 13, where mutual inductance M is added to the ESL of a capacitor. Depending on the winding directions of the inductor, M can be positive or negative [9]. f_0 is the self-resonant frequency of the capacitor; f_1 is the series resonant frequency when $M > 0$; f_2 is the series resonant frequency when $M < 0$ and $|M| < \mathrm{ESL}$; f_3 is the minimum-impedance frequency of the capacitor branch when $M < 0$ and $|M| > \mathrm{ESL}$; f_3 is different from the resonant frequencies because no phase polarity change occurs [9]; f_1, f_2 and f_3 are given by

$$f_1 = \frac{1}{2\pi\sqrt{(ESL+M)C}} \tag{12}$$

$$f_2 = \frac{1}{2\pi\sqrt{(ESL-M)C}} \quad \text{and} \tag{13}$$

$$f_3 = \frac{1}{2\pi\sqrt{(M-ESL)C}}. \tag{14}$$

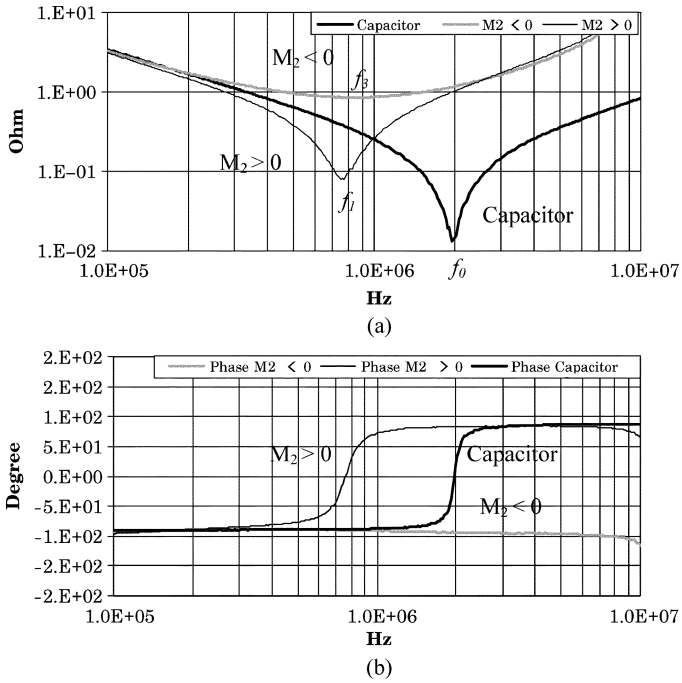

Fig. 14. Derived impedances for the C_1 branch from the measured S-parameters: (a) magnitude and (b) phase.

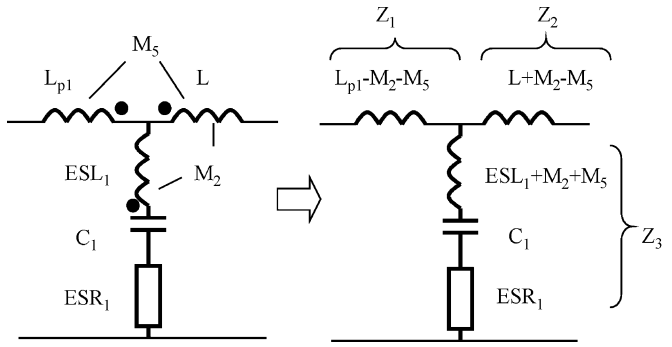

Fig. 15. Calculation of M_5 through the impedance of the capacitor branch.

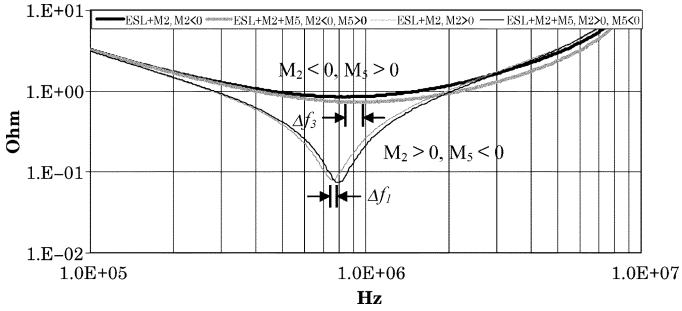

Fig. 16. Derived impedances of the C_1 branch from measured S-parameters.

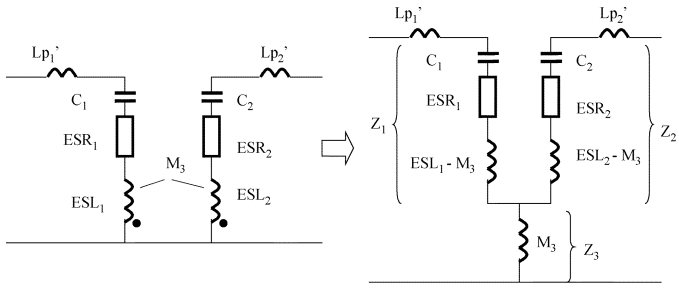

Fig. 17. Equivalent circuit for the inductive coupling between two capacitors.

In the circuit shown in Fig. 9, in order to find M_2, the S-parameters of the network including one capacitor and the inductor are measured, and then the impedances of the capacitor branch are derived through (11). The calculated impedance is shown in Fig. 14, where one curve is the capacitor impedance, another curve is the impedance curve when M_2 is positive (inductor winding direction1), and the last one is the impedance curve when M_2 is negative (inductor winding direction2). The self-resonant frequency f_0 of the capacitor is 1.97 MHz. From Fig. 14, when M_2 is positive the resonant frequency f_1 decreases to 747 kHz. When M_2 is negative, the frequency f_3 of the minimum impedance is 850 kHz. Because the capacitance is 0.4667 μF and the ESL is 14 nH, the mutual inductances are calculated using (12)–(14). For the case of $M_2 > 0$, (12) is used for the calculation. M_2 is found to be 83.3 nH. For f_3, since no phase polarity change occurs, based on (14), the M_2 is -89.3 nH. Because of the symmetrical PCB layout, M_1 is equal to M_2.

In order to determine M_4 and M_5, the related in or out trace loop is changed back to their original statuses. The equivalent circuit for M_5 and M_2 is shown in Fig. 15. In Fig. 15, M_2 is already known. Depending on the winding directions of the inductor, M_5 can be positive or negative. In Fig. 16, the derived impedance curves are compared with the previous case shown in Fig. 14. M_5 is then calculated using (12)–(14). In Fig. 16, when M_2 is negative, the frequency of the minimum impedance increases from 850 kHz to 980 kHz, which means M_5 is $+18.7$ nH. When M_2 is positive, the resonant frequency increases from 747 kHz to 790 kHz, which means M_5 is -10.3 nH. M_4 is equal to M_5.

2) Extraction of M_3 and M_6 in Fig. 3: In Fig. 3, in order to extract the mutual inductance M_3 between two capacitors, the inductor is disconnected from the filter, but still remains on the PCB because it affects the inductive couplings in the filter. The in and out trace loops are reduced very small, so the inductive coupling M_6 between them is very small and its effect is ignored. The effect of $C_{\rm p}$ is also ignored because of the small impedances of the two capacitors. The circuit is then simplified as shown in Fig. 17. In Fig. 17, $L'_{\rm p1}$ and $L'_{\rm p2}$ are the inductances of the modified trace loops. The circuit is decoupled into a Tee network. The mutual inductance is transformed to the shunt branch, which corresponds to Z_3 in Fig. 10. M_3 is then determined from Z_3. Fig. 18 shows the Z_3 derived from measured S-parameters. The noise before 500 kHz is the noise floor of the network analyzer. The mutual inductance is finally calculated from Fig. 18 as 0.45 nH. After changing the in and out trace loops back to their original statuses, M_6 can also be derived. Fig. 19 shows the equivalent circuit, and Fig. 20 shows the derived impedance. From Fig. 20, M_6 is 0.2 nH.

3) Extraction of M_7 and $C_{\rm p}$ in Fig. 3: M_7 and $C_{\rm p}$ can be derived by comparing the parallel resonant frequencies of inductor impedance with the derived impedance of the inductor branch. By leaving only the inductor on the PCB and measuring

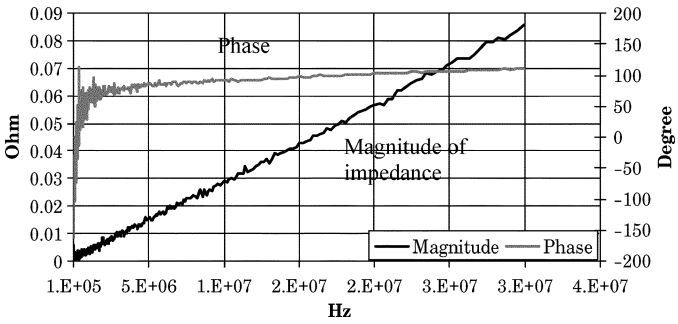

Fig. 18. Impedance of the Z_3 branch, derived from measured S-parameters.

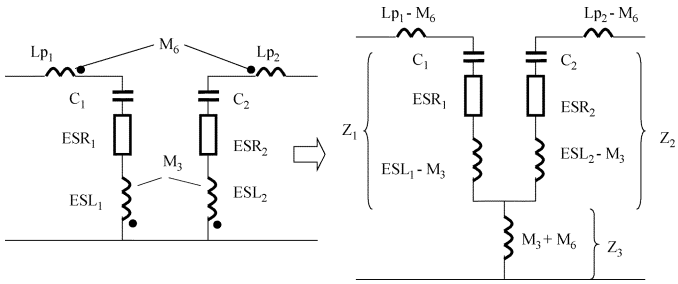

Fig. 19. Equivalent circuit for the inductive couplings between two capacitors and between trace loops.

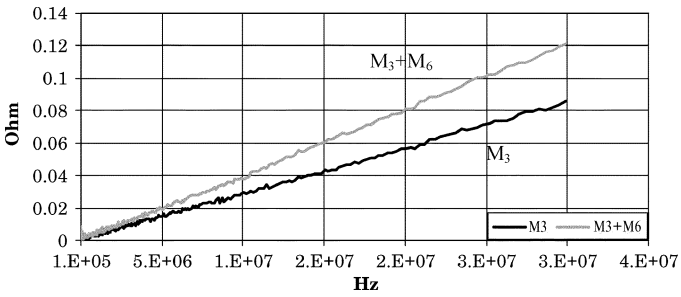

Fig. 20. Derived impedances of the Z_3 branch.

the S-parameters of the circuit, the impedance of the inductor branch can be found as

$$Z_L = 2Z_0\left(\frac{1}{S_{21}} - 1\right). \tag{15}$$

The inductor impedance and the derived impedance of the inductor branch are shown in Fig. 21. From the impedance curves illustrated in Fig. 21, the resonant frequency of the inductor is 14.14 MHz, while the resonant frequency of the inductor branch is 10.5 MHz. From the impedances before 6 MHz, it is obvious that the inductance decreased from 18.91 μH to 18.1 μH. Therefore, M_7 is 0.8 μH, and $C_{\rm p}$ is found to be 5.8 pF.

C. Extraction of Parasitic Parameters for a Two-Stage EMI Filter

Since two-stage EMI filters are widely used in power electronics area, it is necessary to investigate them. Fig. 22 shows a two-stage DM EMI filter, and its PCB layout is shown in Fig. 23. For this two-stage DM EMI filter, the in and out trace loops are very small, so the couplings related to them are ignored. Because the two-stage filter has five components, there

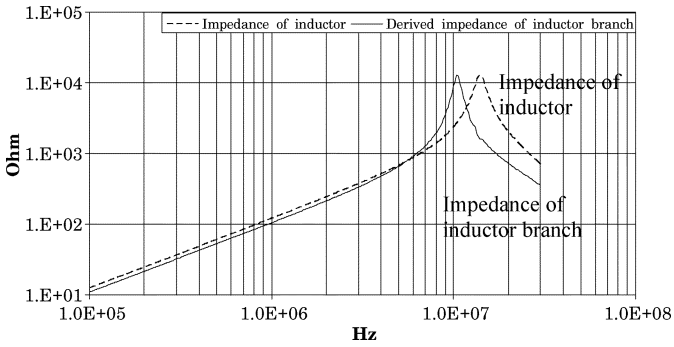

Fig. 21. Impedances of the inductor and the inductor branch.

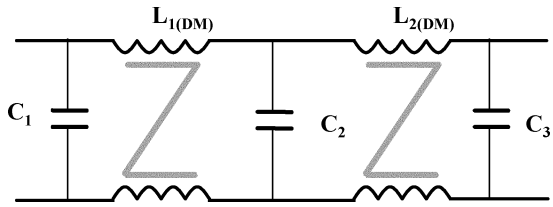

Fig. 22. Investigated two-stage DM EMI filter.

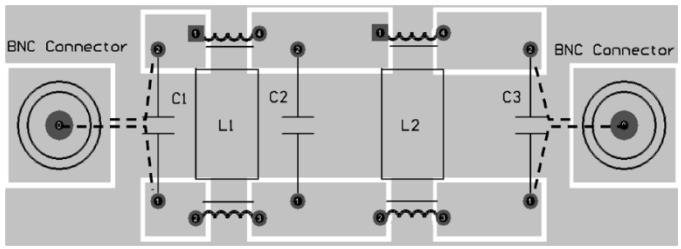

Fig. 23. PCB layout of the investigated two-stage EMI filter.

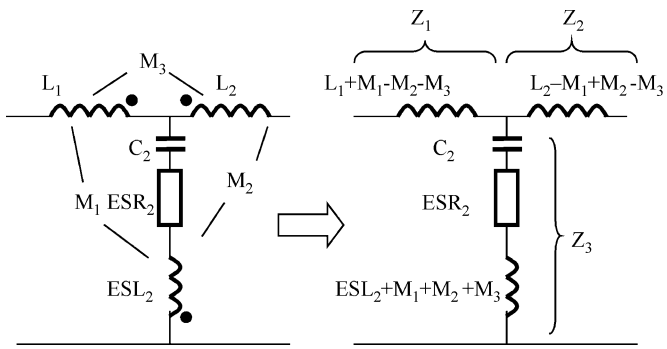

Fig. 24. Equivalent circuit for the inductive couplings between two inductors and between inductors and the capacitor C2.

are 10 mutual couplings among them. All the couplings are extracted using methods similar to those of one-stage filters except the coupling between the two inductors, which is illustrated in Fig. 24. In Fig. 24, M_1 and M_2 have been extracted by the same method as was used for one-stage EMI filters. The impedance of capacitor branch Z_3 is extracted and shown in Fig. 25.

In Fig. 25, the series resonant frequency f_1 of the capacitor branch is 230 kHz, which is much smaller than the 1.72 MHz of the capacitor. This difference is caused by mutual inductances M_1, M_2 and M_3. M_3 is then found, since M_1 and M_2 are already known. M_1 is 88.1 nH, M_2 is 44.3 nH, and M_3 is found as 0.908 μH.

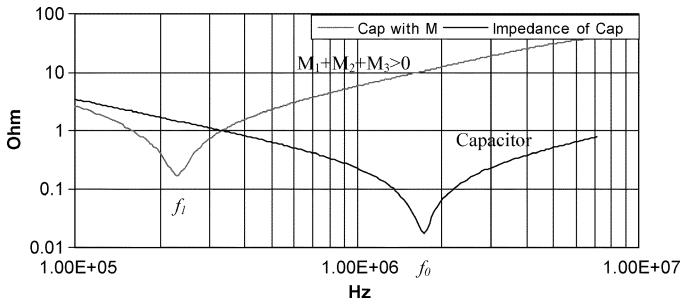

Fig. 25. Derived impedances of the C_2 branch from measured S-parameters.

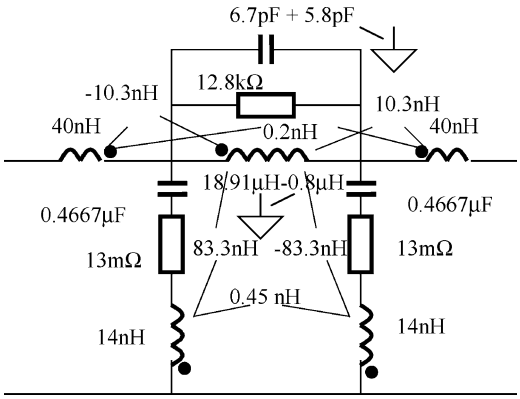

Fig. 26. EMI filter model for inductor winding direction1.

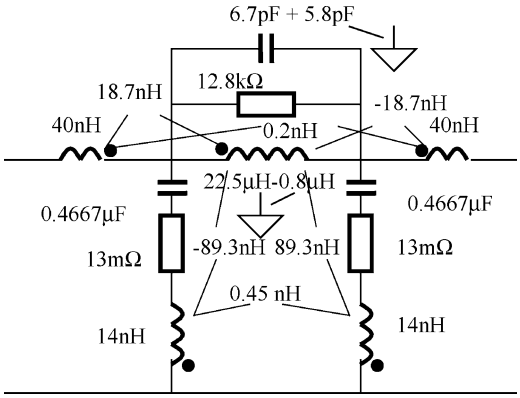

Fig. 27. EMI filter model for inductor winding direction2.

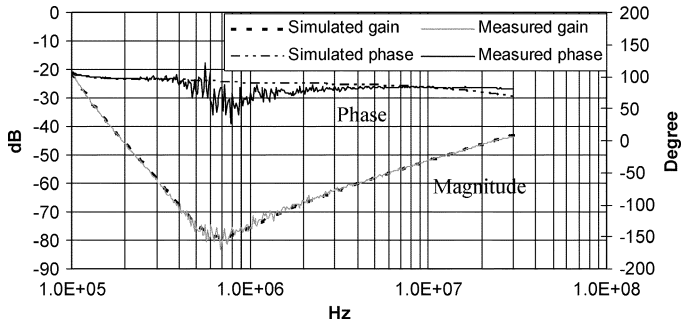

Fig. 28. Comparison of the measured and simulated insertion voltage gains for inductor winding direction1.

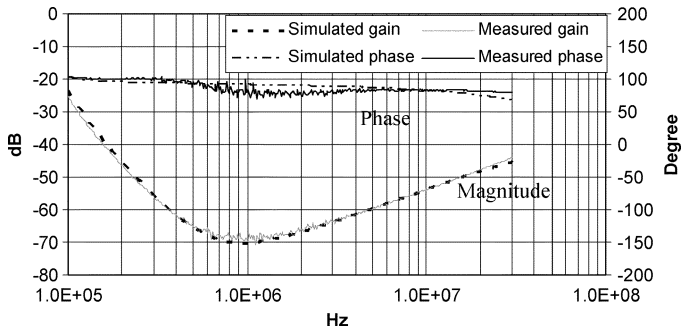

Fig. 29. Comparison of the measured and simulated insertion voltage gains for inductor winding direction2.

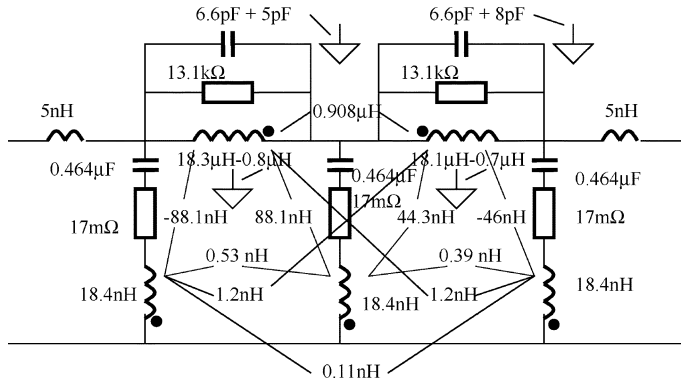

Fig. 30. Two-stage EMI filter model.

IV. Experimental Verification

Since all the parasitic couplings are extracted, it is possible to build and verify EMI filter models. Based on the models, parametric study can be carried out to find the critical couplings for the HF performance of EMI filters.

A. One-Stage EMI Filter

The final filter models for one-stage EMI filters are shown in Figs. 26 and 27. In Figs. 28 and 29, the simulated insertion voltage gains with 50 Ω source and load impedances are compared with the measured results. It is obvious that they match very closely, which verifies the extraction of mutual parasitic parameters. Further parametric study on the models shows the parasitic couplings between the two capacitors and between the inductor and capacitors are critical to the HF performance of EMI filters. This can be explained by the large current difference on two capacitor branches [9] and the large mutual inductance, which is several times larger than the ESL of capacitors, between the inductor and capacitors. The methods to control these couplings and therefore improve the filter HF performance are introduced in [12].

B. Two-Stage EMI Filter

The final two-stage EMI filter model is shown in Fig. 30. The simulated insertion voltage gain when both source and load are 50 Ω is compared with the measured one shown in Fig. 31. In Fig. 31, the simulated and measured curves match very closely; this verifies the extracted parasitic parameters. The noise between 200 kHz and 1 MHz in both pictures is the noise floor

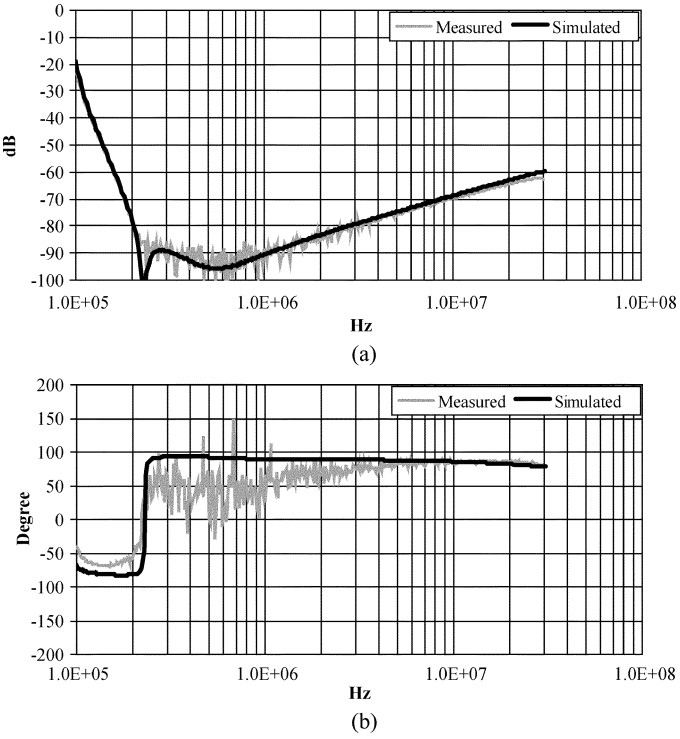

Fig. 31. Comparison of the measured and simulated insertion voltage gains: (a) magnitude and (b) phase.

of the network analyzer. Further parametric study on the model shows the mutual inductance between the two inductors significantly affects the corner frequency of the insertion voltage gain at around 230 kHz. This is because the series resonant frequency of the C_2 branch is greatly lowered by the mutual inductance between two inductors. The parametric study also shows the mutual inductance between C_1 and C_3 significantly affects the insertion voltage gain above 1 MHz. Although this coupling is very small, the large current difference between two capacitor branches makes it very critical. Other couplings such as the mutual inductances between L_1 and C_1, C_2, and between L_2 and C_2, C_3 also affect the HF performance of EMI filters because they affect the performance of capacitors.

V. Conclusion

This work first presented a method for using S-parameters to characterize EMI filters. An equation was developed to describe the insertion voltage gain, so it is possible to predict the EMI filter performance with arbitrary levels of source and load impedances. The approach was verified by measurements. A method that uses S-parameters to extract the parasitic parameters of EMI filters is then proposed for parasitic extraction of both one-stage and two-stage EMI filters. The EMI filter models are built and the extracted parasitic parameters are finally verified by experiments. The constructed filter models are very useful for investigating the effects of parasitic couplings on EMI filter performance, and they therefore offer guidelines for EMI filter design.

References

[1] D. Zhang, D. Y. Chen, and D. Sable, "A new method to characterize EMI filters," in *Proc. IEEE Applied Power Electronics Conf. Expo*, Anaheim, CA, Feb. 15–19, 1998, pp. 929–933.

[2] R. Anderson, Test and Measurement Application Note 95-1 S-Parameters Techniques, Hewlett-Packard, 1997.

[3] Agilent AN154 S-Parameters Design Application Note, Agilent Technologies, 2000.

[4] S. Wang, F. C. Lee, and W. G. Odendaal, "Improving the performance of boost PFC EMI filters," in *Proc. IEEE Applied Power Electronics Conf. Expo*, Miami, FL, Feb. 9–13, 2003, pp. 368–374.

[5] N. Balabanian and T. Bickart, *Linear Network Theory: Analysis, Properties, Design and Synthesis*. New York: Matrix Publishers, Inc., 1981.

[6] S. Wang, F. C. Lee, D. Y. Chen, and W. G. Odendaal, "Effects of parasitic parameters on the performance of EMI filters," in *Proc. IEEE Power Electronics Specialist Conf.*, Acapulco, Mexico, Jun. 15–19, 2003, pp. 73–78.

[7] D. Zhang, D. Y. Chen, M. J. Nave, and D. Sable, "Measurement of noise source impedance of off-line converters," *IEEE Trans. Power Electron.*, vol. 15, no. 5, pp. 820–825, Sep. 2000.

[8] M. W. Medley, *Microwave and RF Circuits: Analysis, Synthesis, and Design*. Boston, MA: Artech House, 1993.

[9] S. Wang, F. C. Lee, D. Y. Chen, and W. G. Odendaal, "Effects of parasitic parameters on the performance of EMI filters," *IEEE Trans. Power Electron.*, vol. 19, no. 3, pp. 869–877, May 2004.

[10] D. H. Liu and J. G. Jiang, "High frequency characteristic analysis of EMI filter in switch mode power supply (smps)," in *Proc. IEEE Power Electronics Specialists Conf.*, vol. 4, 2002, pp. 2039–2043.

[11] S. Wang, F. C. Lee, and W. G. Odendaal, "Using scattering parameters to characterize EMI filters," in *Proc. IEEE Power Electronics Specialists Conf.*, Aachen, Germany, Jun. 20–25, 2004, pp. 297–303.

[12] ——, "Controlling the parasitic parameters to improve EMI filter performance," in *Proc. IEEE Applied Power Electronics Conf.*, vol. 1, Anaheim, CA, Feb. 22–26, 2004, pp. 503–509.

Shuo Wang (S'03) received the B.S.E.E degree from Southwest Jiaotong University, Chengdu, China, in 1994, the M.S.E.E degree from Zhejiang University, Hangzhou, China, in 1997, and is currently pursuing the Ph.D. degree at the Center for Power Electronics Systems (CPES), Virginia Polytechnic Institute and State University, Blacksburg.

From 1997 to 1999, he was with ZTE Telecommunication Corporation, Shenzhen, China, where he was a Senior R&D Engineer and responsible for the development and support of the power supply for wireless products. In 2000, he worked at UTstarcom Telecommunication Corporation, Hangzhou, China, where he was responsible for the development and support of the optical access networks. He has one U.S. patent pending.

Mr. Wang received excellent R&D Engineer Award in 1998.

Fred C. Lee (S'72–M'74–SM'87–F'90) received the B.S. degree in electrical engineering from National Cheng Kung University, Taiwan, R.O.C., in 1968 and the M.S. and Ph.D. degrees in electrical engineering from Duke University, Durham, NC, in 1971 and 1974, respectively.

He is a University Distinguished Professor with Virginia Polytechnic Institute and State University (Virginia Tech), Blacksburg, and prior to that he was the Lewis A. Hester Chair of Engineering at Virginia Tech. He directs the Center for Power Electronics Systems (CPES), a National Science Foundation engineering research center whose participants include five universities and over 100 corporations. In addi-

tion to Virginia Tech, participating CPES universities are the University of Wisconsin-Madison, Rensselaer Polytechnic Institute, North Carolina A&T State University, and the University of Puerto Rico-Mayaguez. He is also the Founder and Director of the Virginia Power Electronics Center (VPEC), one of the largest university-based power electronics research centers in the country. VPEC's Industry-University Partnership Program provides an effective mechanism for technology transfer, and an opportunity for industries to profit from VPEC's research results. VPEC's programs have been able to attract world-renowned faculty and visiting professors to Virginia Tech who, in turn, attract an excellent cadre of undergraduate and graduate students. Total sponsored research funding secured by him over the last 20 years exceeds $35 million. His research interests include high-frequency power conversion, distributed power systems, space power systems, power factor correction techniques, electronics packaging, high-frequency magnetics, device characterization, and modeling and control of converters. He holds 30 U.S. patents, and has published over 175 journal articles in refereed journals and more than 400 technical papers in conference proceedings.

Dr. Lee received the Society of Automotive Engineering's Ralph R. Teeter Education Award (1985), Virginia Tech's Alumni Award for Research Excellence (1990), and its College of Engineering Dean's Award for Excellence in Research (1997), in 1989, the William E. Newell Power Electronics Award, the highest award presented by the IEEE Power Electronics Society for outstanding achievement in the power electronics discipline, the Power Conversion and Intelligent Motion Award for Leadership in Power Electronics Education (1990), the Arthur E. Fury Award for Leadership and Innovation in Advancing Power Electronic Systems Technology (1998), the IEEE Millennium Medal, and honorary professorships from Shanghai University of Technology, Shanghai Railroad and Technology Institute, Nanjing Aeronautical Institute, Zhejiang University, and Tsinghua University. He is an active member in the professional community of power electronics engineers. He chaired the 1995 International Conference on Power Electronics and Drives Systems, which took place in Singapore, and co-chaired the 1994 International Power Electronics and Motion Control Conference, held in Beijing. During 1993-1994, he served as President of the IEEE Power Electronics Society and, before that, as Program Chair and then Conference Chair of IEEE-sponsored power electronics specialist conferences.

Willem Gerhardus Odendaal (M'98) was born in South Africa in 1969. He received the B.Eng., M.Eng., and D.Eng. degrees in electrical and electronics engineering from Rand Arikaans University, Johannesburg, South Africa, in 1992, 1995, and 1997, respectively.

He spent one year in a post-doctoral position under two fellowships at the Virginia Power Electronics Center, Virginia Polytechnic Institute and State University (Virginia Tech), Blacksburg, before joining Philips Research North America in New York as Senior Member of Research Staff. Since Fall 2001, he has been an Assistant Professor in the Bradley Department of Electrical and Computer Engineering, Virginia Tech, as well as a Faculty Member of the NSF Engineering Research Center for Power Electronics Systems (CPES). His research interests include electromagnetic and thermodynamic energy processing and packaging of power electronic circuits.

Dr. Odendaal is a Chairman of the Power Electronics Devices and Components Committee, IEEE Industry Applications Society.